remote sensing

MDPI

Article

SLR Validation and Evaluation of BDS-3 MEO Satellite Precise Orbits

Ran Li [1,2], Chen Wang [3], Hongyang Ma [4,*], Yu Zhou [2], Chengpan Tang [5], Ziqian Wu [1], Guang Yang [2] and Xiaolin Zhang [6]

1 State Key Laboratory of Satellite Navigation System and Equipment Technology, Shijiazhuang 050081, China; liran@aircas.ac.cn (R.L.); ziqian2009@163.com (Z.W.)
2 Aerospace Information Research Institute (AIR), Chinese Academy of Sciences (CAS), Beijing 100094, China; zhouyu@aircas.ac.cn (Y.Z.); yangguang@aircas.ac.cn (G.Y.)
3 School of Geological Engineering and Geomatics, Chang'an University, Xi'an 710064, China; chen.wang@chd.edu.cn
4 School of Geomatics Science and Technology, Nanjing Tech University, Nanjing 210037, China
5 Shanghai Astronomical Observatory, Chinese Academy of Sciences, Shanghai 200030, China; cptang@shao.ac.cn
6 Beijing Satellite Navigation Center, Beijing 100094, China; xiaolinzhang0924@163.com
* Correspondence: mahongyang@njtech.edu.cn

Abstract: Starting from February 2023, the International Laser Ranging Service (ILRS) began releasing satellite laser ranging (SLR) data for all BeiDou global navigation satellite system (BDS-3) medium earth orbit (MEO) satellites. SLR data serve as the best external reference for validating satellite orbits, providing a basis for comprehensive evaluation of the BDS-3 satellite orbit. We utilized the SLR data from February to May 2023 to comprehensively evaluate the orbits of BDS-3 MEO satellites from different analysis centers (ACs). The results show that, whether during the eclipse season or the yaw maneuver season, the accuracy was not significantly decreased in the BDS-3 MEO orbit products released from the Center for Orbit Determination in Europe (CODE), Wuhan University (WHU), and the Deutsches GeoForschungsZentrum (GFZ) ACs, and the STD (Standard Deviation) of SLR residuals of those three ACs are all less than 5 cm. Among these, CODE had the smallest SLR residuals, with 9% and 12% improvement over WHU and GFZ, respectively. Moreover, the WHU precise orbits exhibit the smallest systematic biases, whether during non-eclipse seasons, eclipse seasons, or satellite yaw maneuver seasons. Additionally, we found some BDS-3 satellites (C32, C33, C34, C35, C45, and C46) exhibit orbit errors related to the Sun elongation angle, which indicates that continued effort for the refinement of the non-conservative force model further to improve the orbit accuracy of BDS-3 MEO satellites are in need.

Keywords: SLR; BDS-3; precise orbit determination; solar radiation pressure model; eclipse season

Citation: Li, R.; Wang, C.; Ma, H.; Zhou, Y.; Tang, C.; Wu, Z.; Yang, G.; Zhang, X. SLR Validation and Evaluation of BDS-3 MEO Satellite Precise Orbits. *Remote Sens.* **2024**, *16*, 2016. https://doi.org/10.3390/rs16112016

Academic Editor: Jianguo Yan

Received: 26 April 2024
Revised: 26 May 2024
Accepted: 28 May 2024
Published: 4 June 2024

1. Introduction

As an important infrastructure of the Global Navigation Satellite System (GNSS), IGS (International GNSS Service) analysis centers (ACs) provide precise GNSS products to users around the world, including satellite orbit and clock offset. Those products have greatly ensured GNSS high-accuracy applications such as navigation, precise timing, geodynamics, and many other geoscientific research and engineering fields [1,2]. Usually, the differences in data processing strategies and dynamic models used by various IGS ACs lead to variations in the accuracy of individual orbit products, which could lead to inconsistent positioning results for users. Hence, accurately identifying the characteristics of different IGS analysis centers' precise orbits is valuable for users with high-precision positioning needs.

Satellite laser ranging (SLR) has been extensively applied across various geodetic and geophysical fields, significantly enhancing our understanding of the Earth's dynamics.

SLR has been instrumental in determining station positions and velocities [3–5]. It has also contributed to the precise determination of Earth orientation parameters [6,7] and the estimation of tidal parameters [8,9]. Furthermore, SLR data have been crucial for the study of the Earth's gravity field [10,11] and the elasticity of the Earth [12]. This technique has also been employed to observe tectonic plate motions [13,14] and to test relativistic effects [15,16]. Additionally, SLR has provided valuable insights into geocenter motion [17,18] and ocean tide models [19]. Beyond these applications, SLR data are also vital for validating the accuracy of satellite orbits, thereby playing a crucial role in precise orbit determination. This diverse range of applications highlights the comprehensive capabilities of SLR in advancing geodetic and geophysical research.

SLR observations provide an independent validation of the global navigation satellite system (GNSS) orbits derived using microwave measurements [20]. By examining long time series of SLR validation residuals, one can detect deficiencies in the dynamic models used for precise orbit determination (POD) and provide support for improving and refining satellite dynamic models [21].

With the completion of the BeiDou global navigation satellite system (BDS-3), various IGS ACs have incorporated BDS-3 satellites into their precise orbit products. The quality assessment of BDS-3 satellite orbits using SLR data is of significant reference value for enhancing the accuracy of BDS-3 satellite POD, and this procedure becomes practicable since all BDS-3 satellites are equipped with laser retroreflectors. Due to the tracking limitations, the International Laser Ranging Service (ILRS) initially supported SLR observations for only four BDS-3 MEO (Medium Earth Orbit) satellites (C20, C21, C29, and C30). Starting in February 2023, ILRS started to provide SLR data for all 24 BDS-3 MEO satellites. This progression provides favorable conditions for conducting precise orbit assessments of BDS-3 satellites using SLR data.

Many scholars utilize SLR data to analyze the characteristics of GNSS satellite orbits and have also identified issues existing in GNSS satellite orbits. Urschl et al. conducted a study on SLR validation residuals for GPS satellite precise orbits from various IGS ACs and the results indicated that the standard deviation (STD) of SLR residuals from different IGS ACs was approximately within $\pm$3 cm [22]. Montenbruck et al. evaluated 3-month validation results between BDS-2 broadcast ephemeris and SLR data and the results revealed that BDS-2 satellites performed yaw maneuvers during the deep eclipse season when the actual satellite attitude did not align with the nominal attitude [23]. Therefore, the solar radiation pressure (SRP) model established based on the nominal yaw attitude became inappropriate, leading to increased model errors in non-conservative perturbation and subsequently causing a decrease in orbit accuracy. Peng et al. used SLR data to validate the precise BDS-2 orbit products provided by WHU and GFZ from January 2014 to July 2015 [24]. The results show that an obvious orbit accuracy decrease can be observed in both broadcast and precise ephemeris for BDS-2 IGSO/MEO satellites during eclipse seasons, especially the yaw maneuver seasons. Due to the tracking limitations and lack of actual BDS-3 SLR data, scholars have not been able to thoroughly validate the precise orbits of all BDS-3 MEO satellites from different ACs. Therefore, we aim to utilize newly released SLR data to investigate the accuracy of BDS-3 MEO satellite orbits, particularly during the deep eclipse season and satellite yaw maneuver seasons. The objective is to provide valuable insights for further enhancing the precision of BDS-3 MEO satellite orbit determination.

SLR validation residuals can detect deficiencies in the dynamic models used for the POD of satellites and thus provide essential references for refining these satellite dynamic models. Research has indicated that orbit errors in Galileo satellites' SLR residuals significantly depend on the Sun elongation angle when using the Extend CODE Orbit Model (ECOM) SRP model [25]. Li et al. found that some IGS ACs may have modeling defects, including BDS-3 orbits of the GFZ and BDS-2 orbits of the European Space Agency (ESA), inferred from the large RMS of SLR residuals [26]. Several scholars, including Urschl et al. [21], Sosnica et al. [27], Yang et al. [28], and Li et al. [29], have already con-

ducted analyses of the adaptability of dynamic models for GPS, Galileo, and BDS satellites using SLR data. However, up to June 2023, the SLR validation of BDS-3 satellites is limited to only four satellites: C20, C21, C29, and C30. Few scholars have utilized the recently released SLR data to study the characteristics of all 24 BDS-3 MEO satellite orbits. Therefore, we intend to apply the SLR data to further detect deficiencies in the dynamic models by different IGS ACs for all 24 BDS-3 MEO satellites.

In this study, we utilize SLR data to validate the precise BDS-3 orbit products released from CODE, WHU, and GFZ. This article is organized as follows. We first describe the motivation and the study objective in Section 2. The method for validating satellite orbits using SLR data is presented in Section 3. Then, an overview of SLR data and the POD strategies employed by different IGS ACs is provided in Section 4. Next, the statistical results of SLR residuals for BDS-3 MEO satellites from different IGS ACs are presented in Section 5.1. Moreover, the performance of BDS-3 MEO satellite orbits during non-eclipse seasons, eclipse seasons, and satellite yaw maneuver seasons is studied in Section 5.2. Additionally, we analyze the characteristics of orbit errors induced by deficiencies in the non-conservative force model of BDS-3 MEO satellites in Section 5.3. Finally, conclusions and discussions are given in Section 6.

2. Motivation and the Study Objective

In February 2023, ILRS began providing SLR tracking data for all 24 BDS-3 MEO satellites. Previously, SLR data were only available for four BDS-3 satellites: C20, C21, C29, and C30. This recent development offers a unique opportunity to comprehensively evaluate the precision of the BDS-3 MEO satellite orbits and the applicability of orbit dynamic models, particularly the solar radiation pressure models, using high-precision SLR data.

The primary motivation for this research stems from the need to leverage the newly available SLR data to assess the accuracy of BBDS-3 MEO satellite orbits provided by different IGS analysis centers. SLR provides an independent and highly precise means of validating satellite orbits, which is crucial for ensuring the reliability of satellite-based navigation and geodetic applications. By evaluating the precision of these orbits, especially during eclipse seasons, this study aims to identify any significant degradation in accuracy and to assess the suitability of different SRP models used in orbit determination.

The objectives of this study include utilizing the newly released SLR data to validate the accuracy of the precise orbits of BDS-3 MEO satellites provided by various IGS analysis centers and investigating the potential accuracy degradation of these orbits during eclipse seasons. Additionally, this study seeks to evaluate the applicability of different SRP models employed in the orbit determination process. Furthermore, it aims to identify any BDS-3 MEO satellites that exhibit distinct characteristics in their precise orbits compared to others, and to explore the underlying reasons, focusing on the adaptability of the SRP models.

By achieving these objectives, this study will provide valuable insights into the performance and reliability of BDS-3 MEO satellite orbits, enhance the understanding of SRP model applicability, and ultimately contribute to the improvement of satellite orbit determination methodologies.

3. SLR Validation

BDS-3 satellites experience non-eclipse season, eclipse season, and satellite yaw maneuver season. The changes in satellite attitude during different seasons would result in variations in satellite orbit accuracy. We implement SLR to verify the characteristics of the precise orbit of BDS-3 MEO satellites during different seasons. In this section, we first introduce the SLR validation method and then describe the conditions when BDS-3 satellites enter the non-eclipse season, eclipse season, and satellite yaw maneuver season.

3.1. SLR Validation Method

Satellite laser ranging involves measuring the time difference between the moment a ground station emits a laser pulse and the moment the laser pulse returns after being reflected by the satellite retroreflectors. This can be expressed as follows:

$$\rho_0 = \frac{1}{2}c\tau \tag{1}$$

where ρ_0 represents the observed distance, c is the speed of light, and τ is the round-trip time of the laser pulse. The parameter ρ_0 can be further expressed as follows:

$$\rho_0 = \frac{1}{2}(\rho_{up}(t) + \rho_{down}(t)) + \Delta\rho_{rel} + \Delta\rho_{trop} + \Delta\rho_{LRA} + \varepsilon \tag{2}$$

where ρ_{up} and ρ_{down} represent the uplink and downlink distances after accounting for the equation of light corrections, $\Delta\rho_{rel}$ is the distance correction caused by the relativistic effect, $\Delta\rho_{trop}$ is the correction for troposphere delay, $\Delta\rho_{LRA}$ compensates for the deviations between LRA (Laser Retroreflector Array) reference point and signal reflection center, and ε represents the system errors related to the ground station and satellite. In the inertial frame of reference, ρ_{up} and ρ_{down} are represented as follows:

$$\begin{cases} \rho_{up}(t) = \left\| r(t - \tau_{down}) - R(t - \tau_{down} - \tau_{up}) \right\| \\ \rho_{down}(t) = \| r(t - \tau_{down}) - R(t) \| \end{cases} \tag{3}$$

where r and R represent the positions of the satellite and SLR station, τ_{up} is the uplink time, and τ_{down} is the downlink time. Since the positions of the satellite and ground station are typically expressed in the Earth-fixed frame of reference, it is necessary to account for the rotation effect of the Earth and coordinate system transformations [30].

SLR residuals refer to the difference between the observed distance ρ_0 and the calculated distance ρ_c. These SLR residuals reflect satellite orbit errors in the direction of the line of sight from the SLR ground station to the satellite. Considering the SLR errors, applying SLR data for satellite orbit validation follows the following steps. First, we extract the observed distances ρ_0 from the SLR data and apply various error corrections to the observational data, including solid tides, pole tides, ocean tides, atmospheric pressure loads, tropospheric delay, relativistic effects, and LRA offsets. Second, we calculate the satellite-to-ground distances ρ_c in the usage of precise satellite ephemerides. Finally, the difference between the observed distances and calculated distance yields SLR residuals. We conduct a statistical analysis on SLR residual values derived from various ground stations for the same satellite. These SLR residuals serve as an assessment metric for evaluating the precise orbit products.

To avoid the influence of outliers on statistical results, we set reasonable threshold values before performing statistical analysis on SLR residuals. In particular, a threshold of ± 1 m is used for BDS-3 MEO satellites, which helps remove outliers from the SLR results. The dynamic models and observation models applied in SLR validation are detailed in Table 1.

The research method of this article is shown in Figure 1. First, we extracted observation data and meteorological data from the SLR standard point data. This data underwent preprocessing and various error corrections to calculate the observed distance ρ_0. Next, we corrected the SLR station coordinates and combined them with satellite precise orbits to calculate the satellite-to-ground distances ρ_c. This involved using precise ephemerides from different analysis centers such as CODE, WHU, and GFZ, which provide high-accuracy orbital information necessary for computing the expected range between the satellite and the SLR station. Moreover, we computed the differences between the observed distance ρ_0 and the satellite-to-ground distance ρ_c, known as SLR residuals. These residuals were statistically analyzed to assess the accuracy of the BDS-3 MEO satellite orbits. The residuals were evaluated over different time periods, including eclipse and non-eclipse seasons, to

examine any variations in orbit accuracy related to the satellite's attitude control modes during these periods. We also investigate the relationship between SLR residuals of BDS-3 MEO satellites and the Sun elongation angle. The aim is to identify the adaptability of the dynamic models used in POD for BDS-3 MEO satellites.

Table 1. Dynamic models and observation models used in SLR validation.

Models	Reference
N-body gravitation	DE421 [31]
Geopotential	EGM2008 [32]
Solid earth tides	TIDE2000
Pole tide	IERS Conventions 2010 [33]
Ocean tides	FES2004 [34]
Atmospheric tidal loading	IERS Conventions 2010
Troposphere model	Marrini–Murray model [35]
Relativity effect	IERS Conventions 2010
Precession and nutation	IAU2000R06
Polar motion	IERS EOP C04
Reference frame	ITRF2008

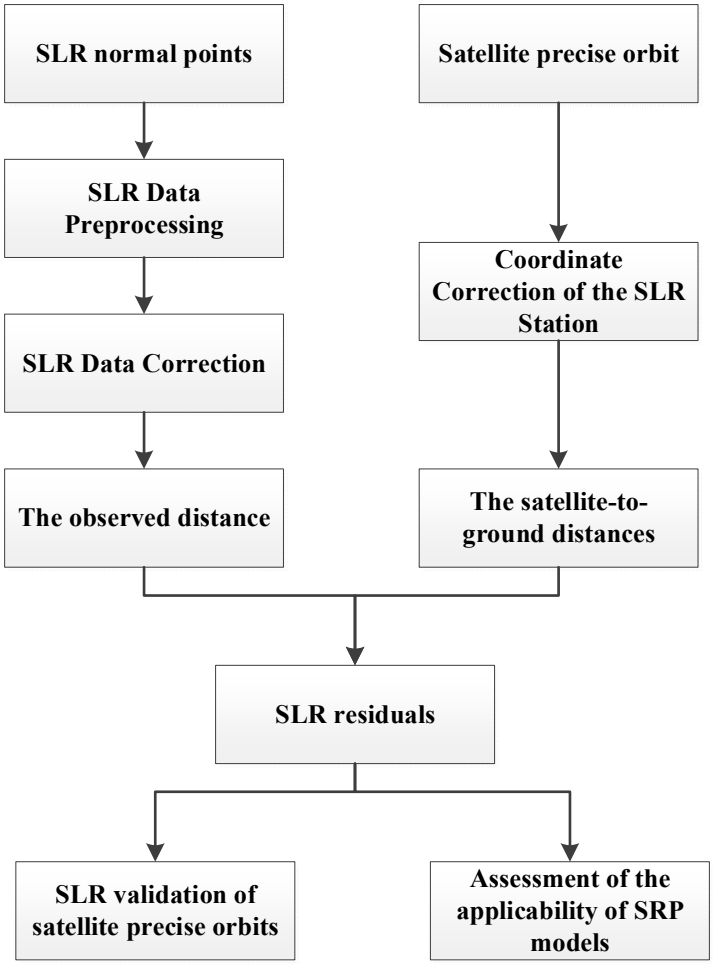

Figure 1. The research methodology of this article.

3.2. Eclipse Season of BDS-3 Satellite

Satellite attitude describes the spatial orientation of the satellite body-fixed frame relative to the inertial frame. Figure 2 illustrates the spatial positions and geometric angles between the Sun, Earth, and satellite. In the satellite body-fixed frame, the *X*-axis and *Z*-axis point towards the Sun and the Earth, respectively, while the *Y*-axis corresponds to the solar panel rotation axis. GNSS satellites are made to comply with the following rules in orbit: First, the satellite antenna should be pointing towards the center of the earth to ensure a sufficient and strong signal reception on the ground; second, the satellite solar panels should be oriented perpendicular to the direction of sunlight, ensuring that in-orbit satellites receive sufficient energy. As a result, the satellite continuously utilizes the satellite attitude control system to adjust its yaw angle.

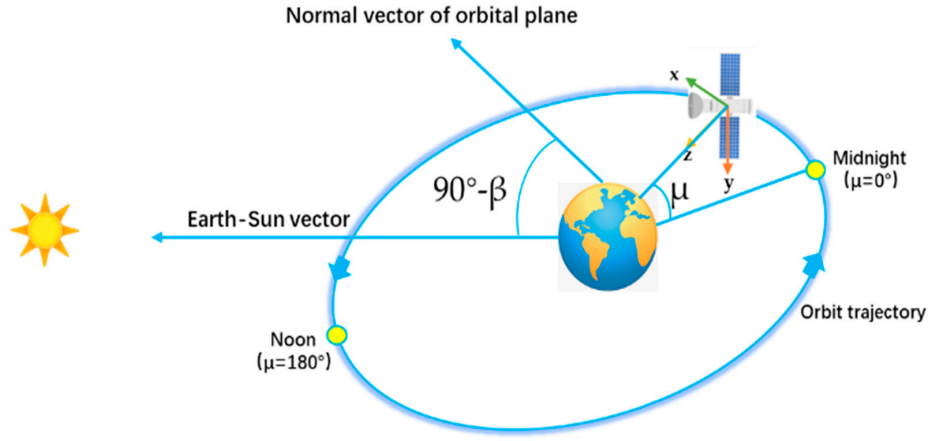

Figure 2. Relationship between the orbital angle μ, solar elevation angle β, and the satellite body-fixed frame.

Sun elongation angle is formed by the Sun–satellite–Earth configuration and is equivalent to the angle between the *z*-axis of the satellite body-fixed frame and the direction of the Sun, which can serve as an effective independent variable for describing the satellite–sun orientation. Therefore, it can be utilized to analyze the characteristics of how solar radiation pressure affects satellite orbit errors. It is worth noting that the satellite-to-Earth distance is only about 0.01% compared to the satellite-to-Sun distance. Hence, it can be assumed that the satellite–Sun vector is parallel to the Earth–Sun vector. Therefore, the Sun elongation angle ε can be expressed in Formula (4) [36]:

$$\cos \varepsilon = \cos \beta \cdot \cos \mu \tag{4}$$

where β represents the angle between the Sun and the satellite orbital plane, which is called the solar elevation angle. μ stands for the angle between the satellite on the orbital plane and the farthest point from the Sun, known as the orbital angle. This indicates that any systematic biases related to β or μ will result in systematic biases in sun elongation angle ε.

The relationship between the orbital angle μ, solar elevation angle β, and the satellite body-fixed frame is depicted in Figure 2, in which the orbit of noon and midnight stand for the points where the Sun is closest and furthest from the satellite.

The process of a satellite entering the shadow of the earth is known as an eclipse season. The β plays a crucial role in determining the time when a satellite enters the eclipse season. Once the β falls below a certain critical value, the satellite will experience an eclipse. The specific angle threshold for entering the eclipse season varies depending on the type of satellite. For instance, GEO (Geostationary Earth Orbit) and IGSO (Inclined Geosynchronous Orbit) satellites of the BeiDou system enter the eclipse season when β is less than 8.7°, while MEO satellites are less than 12.9° [28].

In the eclipse season, especially when β is small, the satellite requires a relatively high rate of attitude adjustment near noon and midnight to maintain the nominal spatial orientation. However, due to the limited hardware adjustment rate of the attitude control momentum wheels, it is often not possible to maintain the in-orbit nominal orientation of the satellite. As a result, the satellite needs to perform yaw maneuvers at a lower rate [37]. In 2019, the China Satellite Navigation Office released preliminary BDS-3 satellite metadata, which mentioned that BDS-3 IGSO/MEO satellites use a Continuous Yaw Steering (CYS) mode during eclipse seasons [38]. Research indicates that BDS-3 MEO satellites switch from yaw steering mode to CYS mode when β falls below 3.4° [39].

4. Data and POD Strategies

In February 2023, the ILRS began releasing SLR data for all BDS-3 MEO satellites, providing a foundation for analyzing the precise orbit characteristics of BDS-3 MEO satellites. Different IGS ACs employ varying satellite orbit determination strategies for BDS-3 MEO satellites, leading to distinct characteristics in the precise orbit products. Therefore, to better understand the precise orbit characteristics of BDS-3 MEO satellites, we first analyze the status of SLR observation stations capable of tracking BDS-3 MEO satellites and then present the LRA information for all BDS-3 MEO satellites. Finally, a detailed description of the satellite orbit determination strategies employed by different IGS ACs is provided.

4.1. Tracking Stations

The ILRS was established in 1998, with a charter to organize and coordinate worldwide satellite laser ranging activities to support programs in geodetic, geophysical, and lunar research activities and to provide the International Earth Rotation Service (IERS) with products important to the maintenance of an accurate International Terrestrial Reference Frame (ITRF) [40]. SLR data can be downloaded from ftp://edc.dgfi.tum.de/pub/slr/data/npt_crd/, accessed on 20 January 2024.

We provide a statistical analysis of SLR observation stations capable of tracking BDS-3 satellites as of June 2023. In the experimental period (from 1 February 2023, to 13 May 2023), 17 SLR stations are capable of receiving BDS-3 satellite-reflected signals. The distribution of these SLR stations is illustrated in Figure 3. Among these stations, the Changchun station has recorded the highest number of normal points, accounting for 23% of the total receptions. Other stations with significant data reception include Shanghai (18%), Yarragadee (17%), and Mount Stromlo (16%). These four stations collectively contribute to 74% of the total data reception. The rest of the stations have very limited normal points, e.g., stations 1873, 1888, 1890, 7110, 7124, and 7249 recorded fewer than 20 normal points during the observational period.

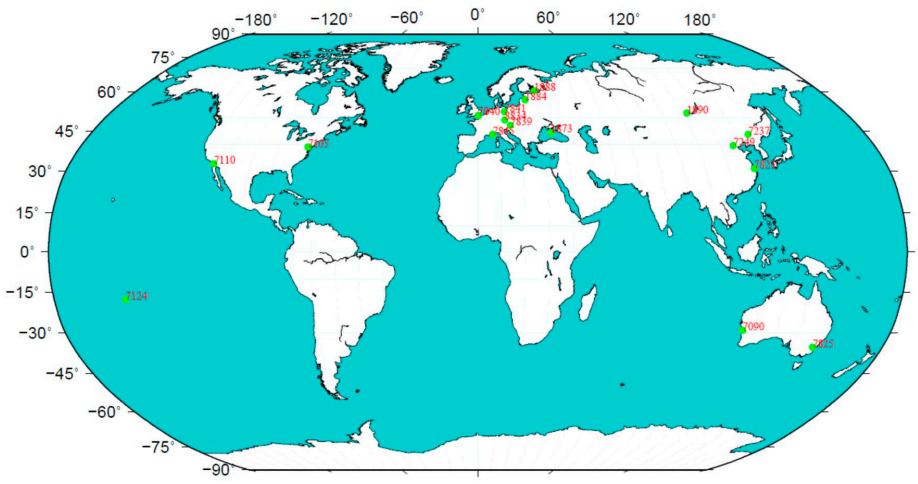

Figure 3. Distribution of the SLR stations that can track BDS-3 satellites.

It is worth noting that during the experimental period, only 2 normal points were observed by the C27 satellite, and the C28 satellite did not observe any normal points. Therefore, C27 and C28 satellites are not included in the statistics for all subsequent experiments.

Table 2 provides a summary of the SLR station information employed in this study, including the detector type, station abbreviation, station location, and the number of available normal points observed by the station during the observational period.

Table 2. SLR station information.

Station	Site Code	Detector Type	Location Name	Country	Available Normal Points
1873	SIML	PMT	Simeiz	Ukraine	7
1884	RIGL	PMT	Riga	Latvia	44
1888	SEVL	PMT	Svetloe	Russia	20
1890	BADL	PMT	Badary	Russia	7
7090	YARL	MCP	Yarragadee	Australia	1087
7105	GODL	MCP	Greenbelt	USA	174
7110	MONL	MCP	Monument Peak	USA	7
7124	THTL	MCP	Tahiti	French Polynesia	18
7237	CHAL	CSPAD	Changchun	China	1421
7249	BEIL	CSPAD	Beijing	China	15
7821	SHA2	CSPAD	Shanghai	China	1119
7825	STL3	CSPAD	Mt Stromlo	Australia	988
7839	GRZL	CSPAD	Graz	Austria	538
7840	HERL	CSPAD	Herstmonceux	United Kingdom	344
7841	POT3	CSPAD	Potsdam	Germany	255
7845	GRSM	CSPAD	Grasse	France	74
8834	WETL	CSPAD	Wettzell	Germany	159

4.2. LRAs Onboard BDS-3 Satellites

SLR technology offers a highly precise and fully independent external method for satellite orbit validation. All BDS-3 satellites are equipped with laser reflector arrays (LRAs), allowing for accurate satellite ranging, which in turn facilitates the assessment of satellite orbit accuracy. SLR observations measure the distance between the ground station and the geometric center of the laser reflector prism on the satellite. Since the precise ephemeris products provide the center of mass coordinates of the satellite, we select the center of mass of the satellite as the reference point and transform the SLR observation data to the geometric center. We utilize the LRA offsets for the BDS-3 satellites, as published by CSNO [38]. These values represent the offset of the LRA relative to the satellite center of mass. Table 3 provides the statistics of the BDS-3 satellites and their corresponding LRA offsets (https://ilrs.gsfc.nasa.gov/missions/satellite_missions/current_missions/bdm2_general.html accessed on 30 March 2024). It should be noted that BDS-3 MEO satellites are produced by two manufacturers, which are the China Academy of Space Technology (CAST) and the Shanghai Engineering Center for Microsatellites (SECM).

Table 3. LRA offsets of BDS-3 MEO satellites.

PRN	ILRS Name	COSPAR ID	Mass (Kg)	Manufacture	X (m)	Y (m)	Z (m)
C19	BDS-3M1	2017-069A	943	BDS-3M-CAST	0.5933	−0.0870	1.2600
C20	BDS-3M2	2017-069B	942	BDS-3M-CAST	0.5947	−0.0846	1.2644
C21	BDS-3M6	2018-018B	942	BDS-3M-CAST	0.5986	−0.0866	1.2650
C22	BDS-3M5	2018-018A	941	BDS-3M-CAST	0.5967	−0.0876	1.2673
C23	BDS-3M9	2018-062A	945	BDS-3M-CAST	0.6045	−0.0809	1.2718
C24	BDS-3M10	2018-062B	946	BDS-3M-CAST	0.6054	−0.0825	1.2628
C25	BDS-3M12	2018-067B	1043.3	BDS-3M-SECM	0.6566	0.4287	0.6100
C26	BDS-3M11	2018-067A	1041.8	BDS-3M-SECM	0.6559	0.4279	0.6092
C27	BDS-3M3	2018-003A	1018	BDS-3M-SECM	0.6096	0.4316	0.6204
C28	BDS-3M4	2018-003B	1014.4	BDS-3M-SECM	0.6080	0.4311	0.6080

Table 3. *Cont.*

PRN	ILRS Name	COSPAR ID	Mass (Kg)	Manufacture	X (m)	Y (m)	Z (m)
C29	BDS-3M7	2018-029A	1010.4	BDS-3M-SECM	0.6095	0.4260	0.6142
C30	BDS-3M8	2018-029B	1008.6	BDS-3M-SECM	0.6097	0.4273	0.6153
C32	BDS-3M13	2018-072A	1007	BDS-3M-CAST	0.6283	−0.0868	1.2367
C33	BDS-3M14	2018-072B	1007	BDS-3M-CAST	0.6276	−0.0882	1.2293
C34	BDS-3M16	2018-078B	1046.6	BDS-3M-SECM	0.6728	0.4282	0.6114
C35	BDS-3M15	2018-078A	1045	BDS-3M-SECM	0.6724	0.4291	0.6095
C36	BDS-3M17	2018-093A	1061	BDS-3M-CAST	0.6133	−0.0892	1.0977
C37	BDS-3M18	2018-093B	1061	BDS-3M-CAST	0.6082	−0.0899	1.0935
C41	BDS-3M19	2019-090A	1059	BDS-3M-CAST	0.6104	−0.0901	1.0924
C42	BDS-3M20	2019-090B	1059	BDS-3M-CAST	0.6084	−0.0893	1.0920
C43	BDS-3M22	2019-078A	1078.8	BDS-3M-SECM	0.6339	0.4250	0.6094
C44	BDS-3M21	2019-078B	1075.4	BDS-3M-SECM	0.6347	0.4248	0.6089
C45	BDS-3M24	2019-061A	1059	BDS-3M-CAST	0.5293	−0.0867	1.1707
C46	BDS-3M23	2019-061B	1058	BDS-3M-CAST	0.5295	−0.0882	1.1634

4.3. MGEX BDS-3 POD Strategies

IGS ACs employ varying SRP models, antenna phase correction information, and GNSS data quality control strategies for different satellites. As a result, the SLR validation residuals of satellite precision orbit products from different ACs will not be the same. Currently, almost all Multi-GNSS Experiment (MGEX) analysis centers can provide precise orbit products for BDS-2 satellites, while WHU, CODE, and GFZ [41–43] offer precise orbit products that include the BDS-3 satellites. Therefore, we primarily selected the BDS-3 precise orbit products from CODE, WHU, and GFZ for our study. To better analyze the characteristics of BDS-3 orbit products released by different ACs, it is essential to understand the orbit determination strategies employed by the corresponding ACs. Table 4 summarizes the dynamic models and orbit determination strategies employed by CODE, WHU, and GFZ [41–44].

Table 4. BDS-3 POD modeling options and estimated parameters of the CODE, WHU, and GFZ.

	CODE	WHU	GFZ
Product	COD	WUM	GBM
Differencing	Double difference	Undifferenced	Undifferenced
Orbit length	72 h	24 h	24 h
Elevation cutoff	3°	10°	7°
Data sampling	5 min	5 min	5 min
Receiver antenna model	igsR3.atx	igs14.atx	igs14.atx
Satellite antenna model	CSNO [38]	igs14.atx	igs14.atx
CAST attitude	Dilssner [45]	Wang et al. [39]	Wang et al. [39]
SECM attitude	Dilssner [45]	CSNO [38]	Zhao et al. [46]
A priori SRP	none	Box wing Wang et al. [47]	none
BDS-3 SRP	EOCM-2 D0, Y0, B0, BC, BS, D2C, D2S	ECOM D0 Y0 B0 BC BS + constant along-track	ECOM D0 Y0 B0 BC BS
Earth albedo	not applied	applied	not applied
Pseudo-stochastic pulses	12 h in R, A, C	not applied	at noon in R, A, C
BDS-3 ambiguity	fix	fix	fix
Software	Bernese GNSS Software 5.3	PANDA	EPOS.P8

5. Results and Analysis

In this section, we utilize SLR data from 1 February 2023, to 13 May 2023, to analyze the orbit accuracy of BDS-3 MEO satellites. First, we conduct an assessment of the orbit accuracy of BDS-3 MEO satellites from different ACs by using SLR data as a reference. Then, we compare the accuracy of precise orbit products from different analysis centers during the non-eclipse seasons, the eclipse seasons, and satellite yaw maneuver seasons. Finally, we analyze the relationship between SLR residuals of BDS-3 MEO satellites and the Sun elongation angle to investigate the adaptability of SRP models further.

5.1. SLR Validation on Precise Orbits of Different IGS ACs

In this study, we conducted an analysis of the precise orbit accuracy of BDS-3 satellites from three IGS Acs—CODE, WHU, and GFZ—utilizing SLR data. The STD of SLR validation residuals represents the stability of satellite orbit, as shown in Figure 4, which illustrates the averaged STD of SLR residuals for BDS-3 MEO satellites from CODE, WHU, and GFZ.

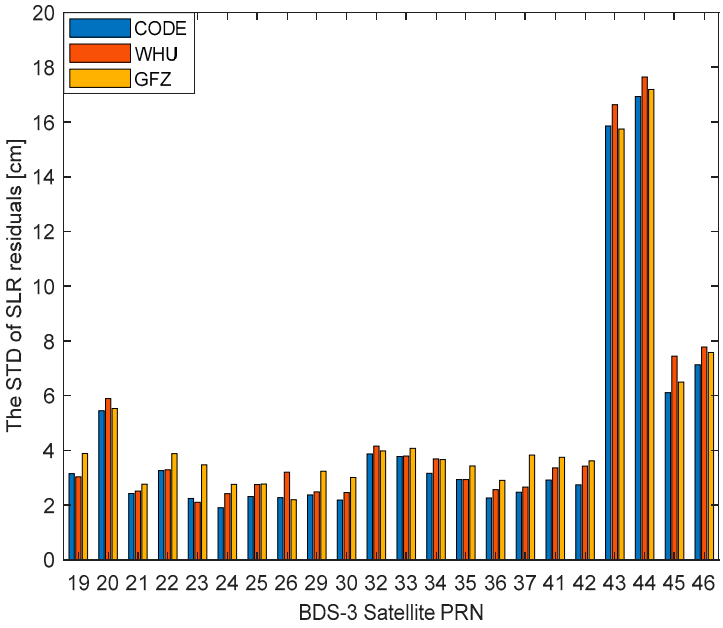

Figure 4. STD of SLR residuals for BDS-3 MEO satellites.

It can be observed in Figure 4 that except for satellites C43 and C44, the STD of SLR residuals for BDS-3 MEO satellite orbits from all three ACs remains within 8 cm, with the majority of satellites having SLR residuals within 4 cm. The STD of SLR residuals for BDS-3 MEO satellite orbits from CODE, WHU, and GFZ are 4.4 cm, 4.8 cm, and 5.0 cm, respectively. Based on the statistical results, it is evident that the precise orbit product stability is the highest at the CODE with an improvement of 9% as compared to WHU and an improvement of 12% as compared to GFZ. The superior performance of the CODE may be attributed to the adoption of the ECOM2 SRP model and the consideration of more non-conservative forces [47,48].

Additionally, it is evident that the orbit accuracy of satellites C43 and C44 is significantly lower than that of other satellites, with the STD of SLR residuals reaching up to 17 cm. In order to better understand the reasons, we have plotted the time series of SLR residuals for satellites C43 and C44. For a visual comparison, we have also plotted the time series of SLR residuals for satellites C36 and C37. The results are presented in Figure 5.

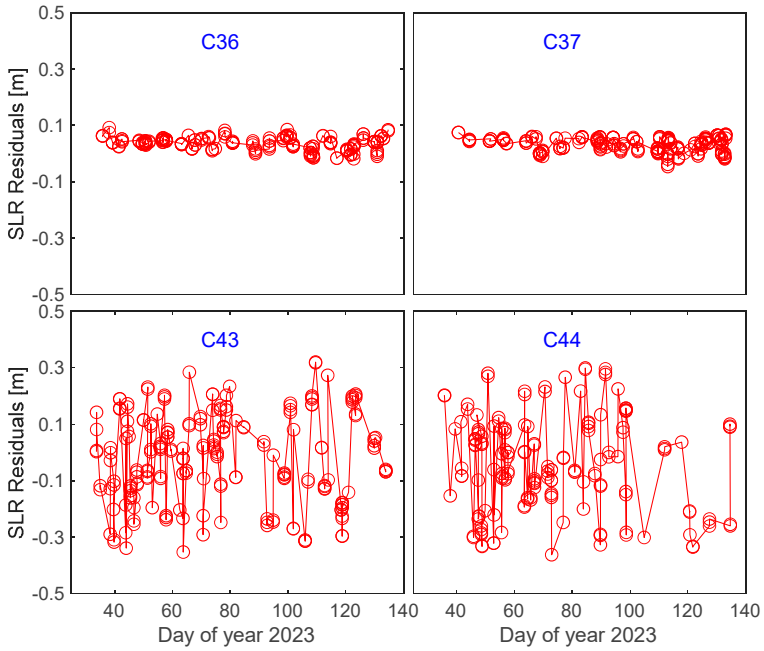

Figure 5. Time series of SLR residuals derived from CODE precise orbits for the BDS-3 satellites C36, C37, C43, and C44.

As shown in Figure 5, the time series of SLR residuals for satellites C36 and C37 exhibit stability, with SLR validation residuals ranging between 0 and 0.1 m. However, in the case of satellites C43 and C44, there is a significant variation in SLR residuals compared to C36 and C37 satellites, with residuals fluctuating within ±0.3 m. The reason for the poor orbit accuracy of satellites C43 and C44 may be associated with inaccuracies in the LRA information provided by the official sources, resulting in an excessive distribution of SLR validation residuals. The underlying cause requires further investigation.

The average SLR residuals represent the magnitude of systematic biases in the validated satellite orbits. In this way, we have compiled the average SLR residuals for BDS-3 MEO satellite orbits from CODE, WHU, and GFZ. Figure 6 presents the average SLR residuals from CODE, WHU, and GFZ.

It can be observed in Figure 6 that the absolute values of the average SLR residuals for BDS-3 MEO satellites from CODE, WHU, and GFZ are 3.6 cm, 3.2 cm, and 3.7 cm, respectively. WHU exhibits the smallest average SLR residuals in precise orbit products, with an improvement of 13% compared to CODE and 14% compared to GFZ. The superior performance of the WHU can be attributed to the consideration of additional non-conservative forces in satellite POD, such as the inclusion of Earth albedo radiation pressure, which mitigates systematic biases in satellite orbits [41]. Furthermore, studies have indicated that the usage of BDS-3 metadata-based or a priori box wing along with empirical ECOM models can reduce systematic modes of SLR residuals [49,50]. Hence, it can be seen that the precise orbit product of WHU has the smallest average SLR residuals.

Furthermore, Figure 6 indicates that the average residuals for BDS-3 CAST satellites (excluding C32 and C33) are positive, while those for SECM satellites exhibit negative values. The possible reason may be related to the fact that C32 and C33 satellites appear to have an additional Earth-facing surface accommodating SAR (Search and Rescue) antennas [51], which results in a configuration inconsistency with other CAST satellites, thus leading to opposite signs in their average residuals. The sign reversal in the average SLR residuals between CAST and SECM satellites may be attributed to the different stretched surfaces for the SECM and CAST satellites [41]. The average residuals for SECM satellites from CODE, WHU, and GFZ are consistently negative. This indicates a stable negative systematic bias between the SECM satellite orbits and SLR observations for CODE, WHU, and GFZ. This bias is likely associated with the use of uncalibrated Earth albedo radiation

models, antenna thrust, and inaccurate modeling of other non-conservative forces within the orbit determination strategy [52].

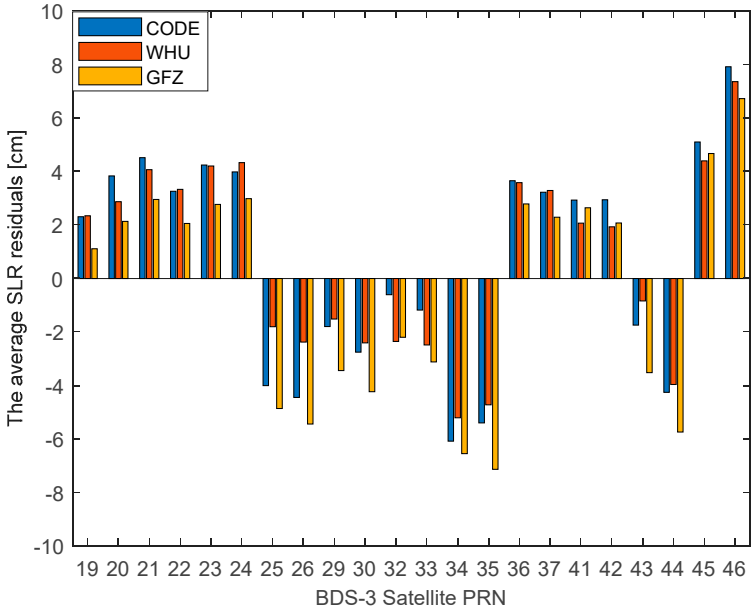

Figure 6. Average SLR residuals for BDS-3 MEO satellites.

5.2. Orbit Accuracy during Different Seasons

In our study, the satellite SLR validation results are categorized based on the non-eclipse season, the eclipse season, and the satellite yaw maneuver season, aiming to further investigate the accuracy of BDS-3 precise orbit products during different seasons. The following criteria were applied in the experiments [39]: when $|\beta| > 12.97°$, BDS-3 MEO satellites are in the non-eclipse season; when $|\beta| < 3.4°$, BDS-3 MEO satellites are in the yaw maneuver season; and when $3.4° \leq |\beta| \leq 12.97°$, BDS-3 MEO satellites are in the eclipse season.

Taking the CODE precise orbit products as an example, we analyze the orbit accuracy of BDS-3 MEO satellites during non-eclipse seasons, eclipse seasons, and satellite yaw maneuver seasons. During the experimental period, a total of eight BDS-3 satellites, namely C23, C25, C26, C29, C30, C34, C35, and C37, transitioned through the eclipse seasons. Therefore, these eight satellites are selected as the subjects of our experiment. We chose four typical satellites, namely C23, C29, C30, and C37, to create time series of SLR validation residuals. Among these, C23 and C37 are CAST satellites, while C29 and C30 are SECM satellites.

From Figure 7, it can be observed that both CAST and SECM satellites do not exhibit a significant decrease in orbit accuracy during the eclipse season compared to the non-eclipse season, indicating that the satellite attitude control strategy adopted by BDS-3 has effectively improved the issue of orbit accuracy degradation during eclipse seasons.

We analyzed the number of SLR normal points for the 8 BDS-3 MEO satellites involved in the experiment during different seasons. The results of the statistics show that the number of SLR normal points during non-eclipse seasons, eclipse seasons, and satellite yaw maneuver seasons are 1155, 557, and 278, respectively. Table 5 presents the SLR orbit validation accuracy of CODE, WHU, and GFZ precise orbit products during non-eclipse, eclipse, and satellite yaw maneuver seasons.

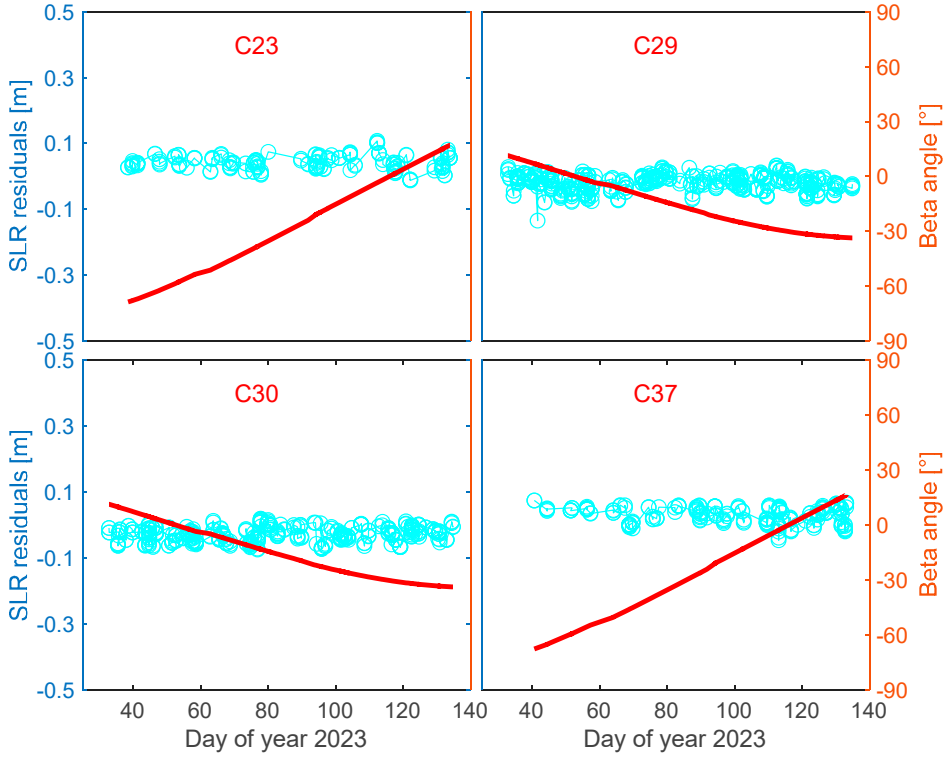

Figure 7. SLR residuals of BDS-3 CAST (C23 and C37) and BDS-3 SECM (C29 and C30) with respect to β (the red line indicates the β).

Table 5. SLR residuals of CODE, WHU, and GFZ precise orbit products during non-eclipse seasons, eclipse seasons, and satellite yaw maneuver seasons (unit: cm).

		CODE	WHU	GFZ
Non-eclipse	STD	2.35	2.70	2.69
	MEAN	3.78	2.91	4.27
Eclipse	STD	2.86	2.49	3.29
	MEAN	4.06	3.37	4.57
Satellite yaw maneuver	STD	2.25	2.40	3.35
	MEAN	4.00	3.00	4.47

Table 5 shows that compared to the SLR validation residuals of BDS-3 MEO satellite orbit from the three IGS ACs, the accuracy of the GFZ precise orbit experiences the most significant degradation during eclipse seasons and yaw maneuver seasons. Furthermore, the statistical results indicate that the precise orbits of CODE and WHU do not exhibit a significant deterioration in orbit accuracy during deep eclipse seasons compared to non-eclipse seasons; instead, the STD of SLR residuals is improving. The possible reason lies in the attitude control mode of BDS-3 satellites during deep eclipse seasons in which the BDS-3 MEO satellite switches to the CYS mode, replacing the orbit normal (ON) mode implemented by BDS-2 MEO satellites. BDS-3 MEO satellites maneuver during deep eclipse seasons when β is within $[-3°, 3°]$ and μ is in the range of approximately $[-6°, 6°]$ or $[174°, 186°]$, occurring near the "Noon" and "Midnight" points [39]. This period lasts for less than an hour each day. In contrast, orbit determination often involves the use of one or three days of arc segments. Therefore, the precise orbits of BDS-3 MEO satellites do not exhibit a significant decrease in accuracy during deep eclipse seasons.

Additionally, it is evident that the WHU precise orbits exhibit the smallest systematic biases since the average SLR residuals are the smallest, whether during eclipse seasons

or non-eclipse seasons. This is attributed to the usage of a more refined non-conservative force model in the WHU POD strategy [41]. When considering the STD of SLR residuals, CODE orbit accuracy for BDS-3 MEO satellites is superior to that of WHU and GFZ during non-eclipse seasons and yaw maneuver seasons. The potential reason is that CODE uses a three-day arc segment orbit determination strategy, which improves the stability of their orbits compared to the one-day orbit determination strategy employed by WHU and GFZ. However, during eclipse seasons, the orbit accuracy of CODE is inferior to that of WHU. The reason may be that WHU employs the a priori box wing along with the empirical ECOM1 model [41], which is more effective at adapting to eclipse seasons.

5.3. Sun-Elongation-Angle-Dependent Systematic Errors

Considering that the Sun elongation angle can serve as an effective independent variable describing the satellite–Sun position, it can be utilized to effectively analyze the characteristics of orbit errors induced by deficiencies in the SRP model [47]. We investigate the relationship between SLR residuals of BDS-3 MEO satellites and the Sun elongation angle. The aim is to identify the adaptability of the dynamic models used in POD for BDS-3 MEO satellites.

We conducted experiments using the BDS-3 precise orbits provided by CODE. Six satellites, namely C20, C21, C24, C25, C29, and C30, were selected for analysis. Among which, C20, C21, and C24 are CAST satellites, while C25, C29, and C30 are SECM satellites. Figure 8 shows the SLR residuals as a function of the Sun elongation angle for the six satellites. As expected, SLR residuals show an obvious linear systematic error with respect to the Sun elongation angle. The color bar corresponds to the change of β, the green line refers to the regression coefficient of the SLR residuals as a linear function of the Sun elongation angle.

From Figure 8, it can be seen that the slope of SLR residuals with regard to the Sun elongation angle of the six satellites are all below 0.3 mm/°, indicating that the applied SRP model is suitable for POD for these satellites. During our research, we discovered that BDS-3 MEO satellites have larger slopes, including C32, C33, C34, C35, C45, and C46. Among these, C32, C33, C45, and C46 are CAST satellites, while C34 and C35 are SECM satellites. Figure 9 shows the slope of SLR residuals with respect to the Sun elongation angle of C32, C33, C34, C35, C45, and C46.

It can be observed in Figure 9 that the C32 and C33 satellites exhibit significantly larger slopes, reaching -1.190 mm/° and -1.309 mm/°, respectively. Since the CODE precise orbit products are involved in this study, which means that the ECOM2 SRP model is employed for POD, the C32 and C33 satellites based on the ECOM2 SRP model show a significant dependence on the variation of the Sun elongation angle. CSNO demonstrates that satellites C32 and C33, for the first time carry, SAR antennas [51]. Hence, the reason for the larger slopes in the case of C32 and C33 satellites could be that the ECOM2 SRP model may not fully account for the dynamic model deviations caused by the addition of extra SAR antennas on C32 and C33 satellites.

The slopes for C34 and C35 satellites are -0.775 mm/° and -0.740 mm/°, respectively. C34 and C35 satellites belong to the SECM manufactory, and it was also observed in Figure 6 that among all the SECM satellites, C34 and C35 satellites have the highest average SLR residuals. The possible reason could be attributed to the higher thermal radiation of solar panels or the much smaller mass than the published value of C34 and C35 satellites [52]. The underlying cause requires additional investigation.

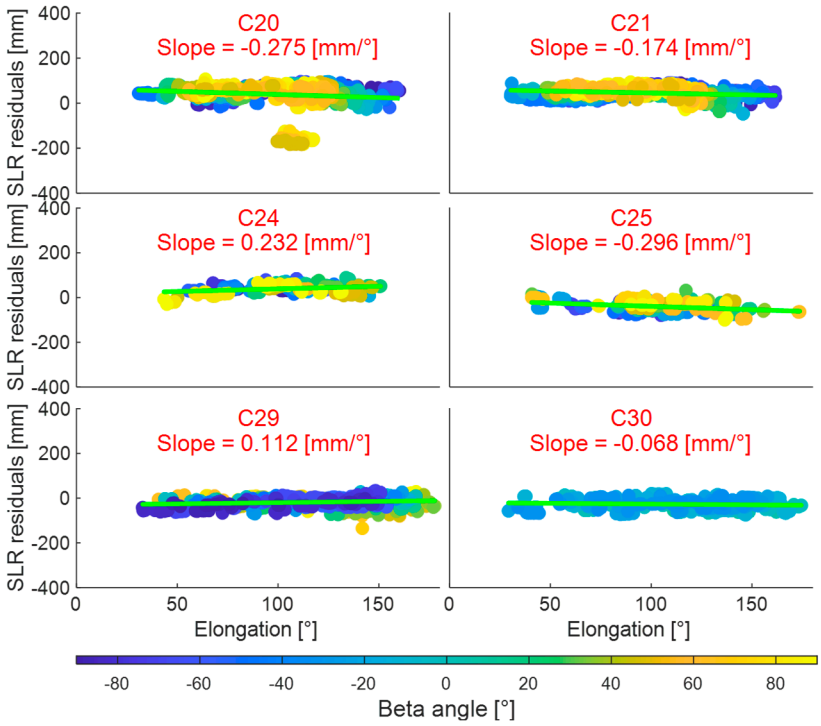

Figure 8. SLR residuals of BDS-3 CAST (C20, C21, and C24) and BDS-3 SECM (C25, C29, and C30) satellites with respect to the Sun elongation angle.

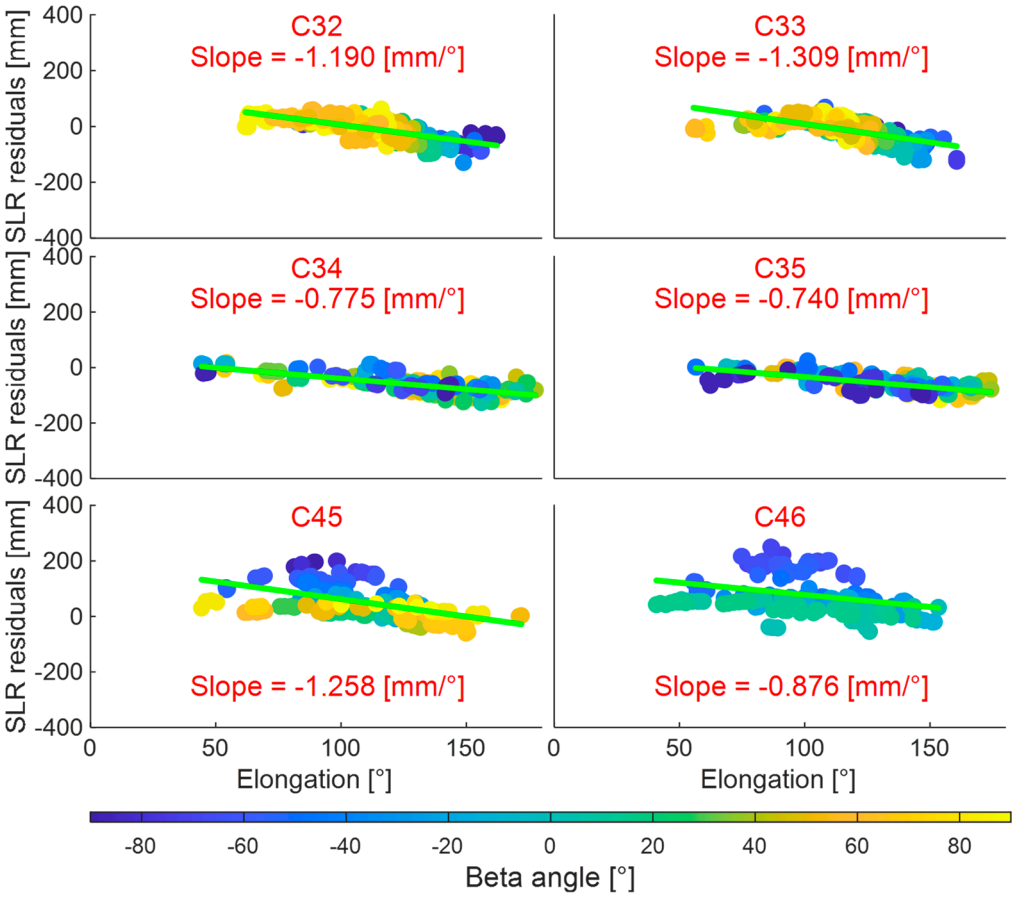

Figure 9. SLR residuals of BDS-3 CAST (C32, C33, C45, and C46) and BDS-3 SECM (C34 and C35) satellites with respect to the Sun elongation angle.

The slopes for C45 and C46 are −1.258 mm/° and −0.876 mm/°, respectively. To investigate the reasons for the large slopes of the C45 and C46 satellites, we plotted the time series of the slope of SLR residuals regarding the β for these two satellites, as shown in Figure 10.

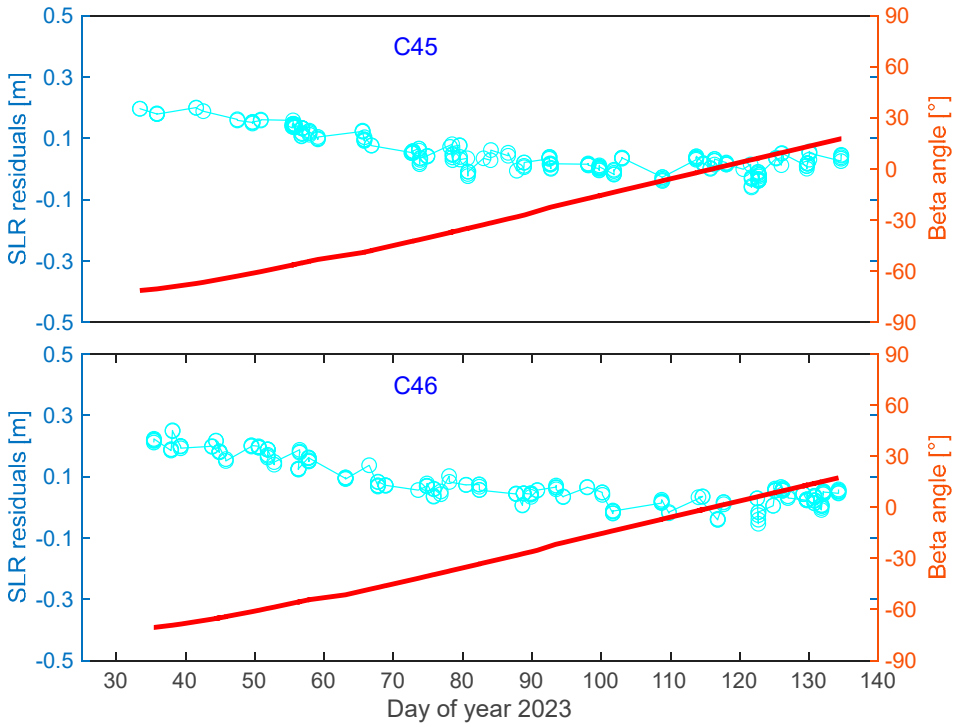

Figure 10. SLR residuals of BDS-3 satellite C45 and C46 with respect to β (the red line indicates β).

As can be seen in Figure 10, unlike other BDS-3 satellites, the SLR residual time series for C45 and C46 exhibit a significant slope and a negative correlation with β. The possible reason is that the C45 and C46 satellites may have a new satellite structure, which results in the SRP model deficiency [53,54].

In order to better study the non-conservative force modeling effect of BDS-3 MEO satellites from CODE, WHU, and GFZ, we selected the precise orbit for BDS-3 MEO satellites from these three IGS ACs and calculated the slope of SLR residuals with regard to the Sun elongation angle. We considered a minimum of 300 observed normal points as a criterion under which eight BDS-3 satellites (C19, C20, C21, C22, C29, C30, C32, and C33) were taken as our study subjects.

For those eight selected BDS-3 MEO satellites in Figure 11, the statistics reveal that the absolute values of the slopes for CODE, WHU, and GFZ are 0.58 mm/°, 0.59 mm/°, and 0.69 mm/°, respectively. CODE and WHU exhibit better slopes, while GFZ has the worst slopes. This indicates that the non-conservative force model, particularly the SRP model, used by CODE and WHU is better suited for BDS-3 MEO satellites. However, the SRP model of GFZ in precise orbit determination requires further refinement.

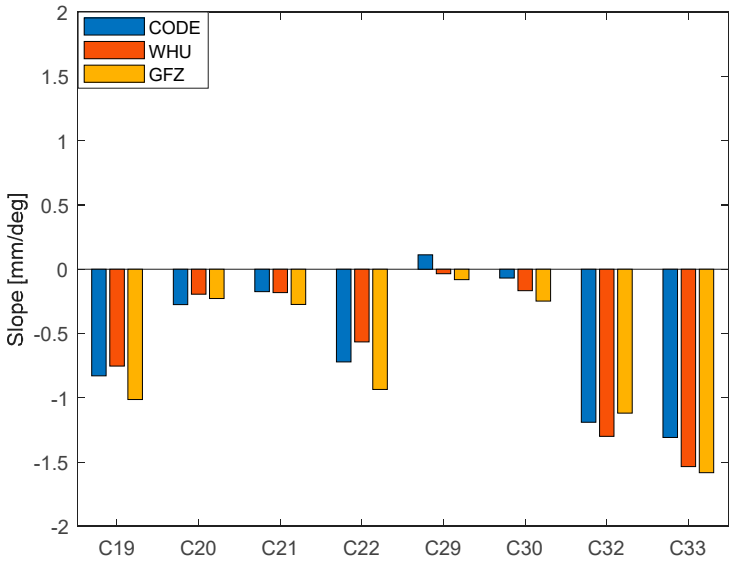

Figure 11. Slope of SLR residuals with respect to the Sun elongation angle.

6. Conclusions

In this contribution, SLR data from 1 February to 13 May 2023 are used to evaluate the precise orbit accuracy of the BDS-3 MEO satellites. The comparative analysis of SLR residuals for BDS-3 MEO satellites from different IGS ACs is presented.

The precise orbits of the BDS-3 MEO satellites from CODE, WHU, and GFZ did not show a significant decrease in orbit accuracy during the eclipse season or the satellite yaw maneuver seasons. The average STD of the SLR residuals for the BDS-3 MEO satellites from CODE, WHU, and GFZ was less than 5 cm, among which the STD of the SLR residuals for the BDS-3 MEO satellite orbit from the CODE was the smallest, with an improvement of 9% and 12% compared with those from WHU and GFZ, respectively. Furthermore, the SLR residuals of C43 and C44 satellites are extraordinarily large, with the STD of SLR residuals reaching up to 17 cm, possibly due to the inaccurate LRA information provided by official sources.

The average SLR residuals, which represent the systematic bias of the orbit, show that the systematic bias of the BDS-3 MEO precise orbits from the WHU is the smallest, regardless of the non-eclipse season, the eclipse season, and the yaw maneuver season. Through POD strategic analysis of the differences among IGS ACs, it can be inferred that utilizing an appropriate non-conservative force model could enhance the accuracy of BDS-3 MEO precise orbits.

We have conducted orbit validation of BDS-3 MEO satellites using SLR data and found that some satellites (C32, C33, C34, C35, C45, and C46) orbit exhibit dynamic model errors related to the Sun elongation angle, which can be attributed to the inadequacy of non-conservative force models and the different satellite structure. Therefore, we must optimize non-conservative force models further, such as the thermal radiation model, to enhance the orbit determination and prediction accuracy of the BDS-3 satellites.

At present, some reasonable conclusions in SLR validation on BDS-3 MEO precise orbits have been demonstrated. The next step is to refine the SRP model for BDS-3 IGSO and MEO satellites, considering the additional antennas and different characteristics of satellite groups.

Author Contributions: R.L. and H.M. wrote the main manuscript text. R.L. and C.W. designed the study. Y.Z. and C.T. performed the experiments. R.L., Z.W., G.Y. and X.Z. analyzed the data. R.L., H.M. and Y.Z. wrote the article. All authors reviewed the manuscript. All authors have read and agreed to the published version of the manuscript.

Funding: This work was supported by the Beijing Natural Science Foundation with Grant No. 1234041, the State Key Laboratory of Satellite Navigation System and Equipment Technology with Grant No. CEPNT2022B01, the National Natural Science Foundation of China (42304025), the Foundation of Science and Technology on Complex Electronic System Simulation Laboratory (614201004022210), the Youth Innovation Promotion Association, CAS (20221276), and the National Key Research Program of China (No. 2022YFC2204700).

Data Availability Statement: Precise satellite orbit products can be found at ftp://igs.ign.fr/pub/igs/products/ and ftp://igs.gnsswhu.cn/pub/gnss/products/mgex/, accessed on 20 January 2024. SLR observation data can be found at ftp://edc.dgfi.tum.de/pub/slr/data/npt_crd/, accessed on 20 January 2024.

Acknowledgments: The authors acknowledge the IGS MGEX and ILRS for providing the multi-GNSS and SLR tracking data.

Conflicts of Interest: The authors declare no conflicts of interest.

References

1. Ma, H.; Li, R.; Tao, J.; Zhao, Q. BDS PPP-IAR: Apply and assess the satellite corrections from different regional networks. *Measurement* **2023**, *211*, 112582. [CrossRef]
2. Li, R.; Zhao, C.; Wu, J.; Ma, H.; Zhang, Y.; Yang, G.; Yuan, H.; Zhao, H. Impacts of Arc Length and ECOM Solar Radiation Pressure Models on BDS-3 Orbit Prediction. *Remote Sens.* **2022**, *14*, 3990. [CrossRef]
3. Lejba, P.; Schillak, S. Determination of station positions and velocities from laser ranging observations to Ajisai, Starlette and Stella satellites. *Adv. Space Res.* **2011**, *47*, 654–662. [CrossRef]
4. Schillak, S.; Lejba, P.; Michałek, P. Analysis of the Quality of SLR Station Coordinates Deter-mined from Laser Ranging to the LARES Satellite. *Sensors* **2021**, *21*, 737. [CrossRef]
5. Strugarek, D.; Sośnica, K.; Arnold, D.; Jäggi, A.; Zajdel, R.; Bury, G. Determination of SLR station coordinates based on LEO, LARES, LAGEOS, and Galileo satellites. *Earth Planets Space* **2021**, *73*, 87. [CrossRef]
6. Shen, Y.; Guo, J.; Zhao, C.; Yu, X.; Li, J. Earth rotation parameter and variation during 2005–2010 solved with LAGEOS SLR data. *Geod. Geodyn.* **2015**, *6*, 55–60. [CrossRef]
7. Strugarek, D.; Sośnica, K.; Arnold, D.; Jäggi, A.; Zajdel, R.; Bury, G.; Drożdżewski, M. Determination of Global Geodetic Parameters Using Satellite Laser Ranging Measurements to Sentinel-3 Satellites. *Remote Sens.* **2019**, *11*, 2282. [CrossRef]
8. Rutkowska, M.; Jagoda, M. Estimation of the elastic Earth parameters (h2, l2) using SLR data. *Adv. Space Res.* **2010**, *46*, 859–871. [CrossRef]
9. Jagoda, M. The evaluation of time variability of tidal parameters h and l using SLR technique. *Acta Geodyn. Geomater.* **2017**, *14*, 153–158. [CrossRef]
10. Cheng, M.K.; Shum, C.K.; Tapley, B.D. Determination of long-term changes in the Earth's gravity field from satellite laser ranging observations. *J. Geophys. Res.* **1997**, *102*, 22377–22390. [CrossRef]
11. Sośnica, K.; Thaller, D.; Jäggi, A.; Dach, R.; Beutler, G. Sensitivity of Lageos Orbits to Global Gravity Field Models. *Artif. Satell.* **2012**, *47*, 47–65. [CrossRef]
12. Rutkowska, M.; Jagoda, M. SLR technique used for description of the Earth elasticity. *Artif. Satell.* **2015**, *50*, 127–141. [CrossRef]
13. Christodoulidis, D.C.; Smith, D.E.; Kolenkiewicz, R.; Klosko, S.M.; Torrence, M.H.; Dunn, P.J. Observing tectonic plate motions and deformations from satellite laser ranging. *J. Geophys. Res.* **1985**, *90*, 9249–9263. [CrossRef]
14. Kraszewska, K.; Jagoda, M.; Rutkowska, M. Tectonic Plate Parameters Estimated in the International Terrestrial Reference Frame ITRF2008 Based on SLR Stations. *Acta Geophys.* **2016**, *64*, 1495–1512. [CrossRef]
15. Ciufolini, I.; Paolozzi, A.; Pavlis, E.; Ries, J.; Gurzadyan, V.; Koenig, R.; Matzner, R.; Penrose, R.; Sindoni, G. Testing General Relativity and gravitational physics using the LARES satellite. *Eur. Phys. J. Plus* **2012**, *127*, 133. [CrossRef]
16. Ciufolini, I.; Paris, C.; Pavlis, E.C.; Ries, J.; Matzner, R.; Paolozzi, A.; Ortore, E.; Bianco, G.; Kuzmicz-Cieslak, M.; Gurzadyan, V.; et al. First results of the LARES 2 space experiment to test the general theory of relativity. *Eur. Phys. J. Plus* **2023**, *138*, 1054. [CrossRef]
17. Matsuo, K.; Otsubo, T.; Munekane, H.; Fukuda, Y. Geocenter motion excited by large-scale mass redistribution. In Proceedings of the 19th International Workshop on Laser Ranging, Annapolis, MD, USA, 27–31 October 2014.
18. Zannat, U.J.; Tregoning, P. Estimating network effect in geocenter motion. *Theory. J. Geophys. Res. Solid Earth* **2017**, *122*, 8360–8375. [CrossRef]
19. Sośnica, K. LAGEOS Sensitivity to Ocean Tides. *Acta Geophys.* **2014**, *63*, 1181–1203. [CrossRef]
20. Tao, E.; Guo, N.; Xu, K.; Wang, B.; Zhou, X. Validation of Multi-Year Galileo Orbits Using Satellite Laser Ranging. *Remote Sens.* **2021**, *13*, 4634. [CrossRef]
21. Urschl, C.; Gurtner, W.; Hugentobler, U.; Schaer, S.; Beutler, G. Validation of GNSS orbits using SLR observations. *Adv. Space Res.* **2005**, *36*, 412–417. [CrossRef]

22. Urschl, C.; Beutler, G.; Gurtner, W.; Hugentobler, U.; Schaer, S. Contribution of SLR tracking data to GNSS orbit determination. *Adv. Space Res.* **2007**, *39*, 1515–1523. [CrossRef]
23. Montenbruck, O.; Steigenberger, P.; Hauschild, A. Broadcast versus precise ephemerides: A multi-GNSS perspective. *GPS Solut.* **2015**, *19*, 321–333. [CrossRef]
24. Peng, H.; Yang, Y.; Wang, G.; He, H. Performance analysis of BDS satellite orbits during eclipse seasons: Results of satellite laser ranging validation. *Acta Geod. Cartogr. Sin.* **2016**, *45*, 639.
25. Montenbruck, O.; Steigenberger, P.; Hugentobler, U. Enhanced solar radiation pressure modeling for Galileo satellites. *J. Geod.* **2015**, *89*, 283–297. [CrossRef]
26. Li, X.; Liu, C.; Yuan, Y.; Zhang, K. Current Status and Challenges of BDS Satellite Precise Orbit Products: From a View of Independent SLR Validation. *Remote Sens.* **2023**, *15*, 2782. [CrossRef]
27. Sośnica, K.; Prange, L.; Kaźmierski, K.; Bury, G.; Drożdżewski, M.; Zajdel, R.; Hadas, T. Validation of Galileo orbits using SLR with a focus on satellites launched into incorrect orbital planes. *J. Geod.* **2018**, *92*, 131–148. [CrossRef]
28. Yang, H.; Xu, T.; Nie, W.; Gao, F.; Guan, M. SLR validation and evaluation on BDS precise orbits from 2013 to 2018. *Adv. Space Res.* **2019**, *64*, 475–490. [CrossRef]
29. Li, X.; Zhu, Y.; Zheng, K.; Yuan, Y.; Liu, G.; Xiong, Y. Precise Orbit and Clock Products of Galileo, BDS and QZSS from MGEX Since 2018: Comparison and PPP Validation. *Remote Sens.* **2020**, *12*, 1415. [CrossRef]
30. Yang, H.; Xu, T.; Nie, W.; Fang, Z.; Li, M.; Guan, M. GLONASS precise orbit determination based on L-band and SLR data. *Meas. Sci. Technol.* **2021**, *32*, 045007. [CrossRef]
31. Folkner, W.M.; Williams, J.G.; Boggs, D.H. The planetary and lunar ephemeris DE 421. *IPN Prog. Rep.* **2009**, *42*, 1–34.
32. Pavlis, N.K.; Holmes, S.A.; Kenyon, S.C.; Factor, J.K. The development and evaluation of the Earth Gravitational Model 2008 (EGM2008). *J. Geophys. Res. Solid Earth* **2012**, *117*. [CrossRef]
33. Petit, G.; Luzum, B. (Eds.) *IERS Conventions 2010, IERS Technical Note 36*; Verlag des Bundesamtes für Kartographie und Geodäsie: Frankfurt, Germany, 2010; 179p, Available online: https://www.iers.org/IERS/EN/Publications/TechnicalNotes/tn36.html (accessed on 20 January 2024).
34. Lyard, F.; Lefevre, F.; Letellier, T.; Francis, O. Modelling the global ocean tides: Modern insights from FES2004. *Ocean Dyn.* **2006**, *56*, 394–415. [CrossRef]
35. Marini, J.W.; Murray, C.W., Jr. Correction of Laser Range Tracking Data for Atmospheric Refraction at Elevations above 10 Degrees (No. NASA-TM-X-70555). 1973. Available online: https://ntrs.nasa.gov/citations/19740007037 (accessed on 20 January 2024).
36. Bar-Sever, Y.E. A new model for GPS yaw attitude. *J. Geod.* **1996**, *70*, 714–723. [CrossRef]
37. Li, X.; Hu, X.; Guo, R.; Tang, C.; Zhou, S.; Liu, S.; Chen, J. Orbit and Positioning Accuracy for New Generation Beidou Satellites during the Earth Eclipsing Period. *J. Navig.* **2018**, *71*, 1069–1087. [CrossRef]
38. China Satellite Navigation Office. CSNO Satellite Information of BDS. Available online: http://en.beidou.gov.cn/SYSTEMS/Officialdocument/201912/P020200103556125703019.rar (accessed on 20 January 2024).
39. Wang, C.; Guo, J.; Zhao, Q.; Liu, J. Yaw attitude modeling for BeiDou I06 and BeiDou-3 satellites. *GPS Solut.* **2018**, *22*, 117. [CrossRef]
40. Pearlman, M.R.; Noll, C.E.; Pavlis, E.C.; Lemoine, F.G.; Combrink, L.; Degnan, J.J.; Kirchner, G.; Schreiber, U. The ILRS: Approaching 20 years and planning for the future. *J. Geod.* **2019**, *93*, 2161–2180. [CrossRef]
41. Guo, J.; Wang, C.; Chen, G.; Xu, X.; Zhao, Q. BDS-3 precise orbit and clock solution at Wuhan University: Status and improvement. *J. Geod.* **2023**, *97*, 15. [CrossRef]
42. Prange, L.; Villiger, A.; Sidorov, D.; Schaer, S.; Beutler, G.; Dach, R.; Jäggi, A. Overview of CODE's MGEX solution with the focus on Galileo. *Adv. Space Res.* **2020**, *66*, 2786–2798. [CrossRef]
43. Deng, Z.; Nischan, T.; Bradke, M. *Multi-GNSS Rapid Orbit-, Clock- & EOP-Product Series*; GFZ Data Services: Potsdam, Germany, 2017. [CrossRef]
44. Steigenberger, P.; Deng, Z.; Guo, J.; Prange, L.; Song, S.; Montenbruck, O. BeiDou-3 orbit and clock quality of the IGS Multi-GNSS Pilot Project. *Adv. Space Res.* **2023**, *71*, 355–368. [CrossRef]
45. Dilssner, F. *A Note on the Yaw Attitude Modeling of BeiDou IGSO-6*; ESA/ESOC Technical Report; European Space Operations Centre: Darmstadt, Germany, 2017.
46. Zhao, Q.; Wang, C.; Guo, J.; Wang, B.; Liu, J. Precise orbit and clock determination for BeiDou-3 experimental satellites with yaw attitude analysis. *GPS Solut.* **2018**, *22*, 4. [CrossRef]
47. Wang, C.; Guo, J.; Zhao, Q.; Liu, J. Empirically derived model of solar radiation pressure for BeiDou GEO satellites. *J. Geod.* **2019**, *93*, 791–807. [CrossRef]
48. Arnold, D.; Meindl, M.; Beutler, G.; Dach, R.; Schaer, S.; Lutz, S.; Prange, L.; Sośnica, K.; Mervart, L.; Jäggi, A. CODE's new solar radiation pressure model for GNSS orbit determination. *J. Geod.* **2015**, *89*, 775–791. [CrossRef]
49. Yan, X.; Liu, C.; Huang, G.; Zhang, Q.; Wang, L.; Qin, Z.; Xie, S. A Priori Solar Radiation Pressure Model for BeiDou-3 MEO Satellites. *Remote Sens.* **2019**, *11*, 1605. [CrossRef]
50. Li, X.; Yuan, Y.; Zhu, Y.; Jiao, W.; Bian, L.; Li, X.; Zhang, K. Improving BDS-3 precise orbit determination for medium earth orbit satellites. *GPS Solut.* **2020**, *24*, 1–13. [CrossRef]
51. Duan, B.; Hugentobler, U.; Selmke, I.; Marz, S.; Killian, M.; Rott, M. BeiDou satellite radiation force models for precise orbit determination and geodetic applications. *IEEE Trans. Aerosp. Electron. Syst.* **2022**, *58*, 2823–2836. [CrossRef]

52. Zhao, Q.; Guo, J.; Wang, C.; Lyu, Y.; Xu, X.; Yang, C.; Li, J. Precise orbit determination for BDS satellites. *Satell. Navig.* **2022**, *3*, 2. [CrossRef]
53. Zajdel, R.; Steigenberger, P.; Montenbruck, O. On the potential contribution of BeiDou-3 to the realization of the ter-restrial reference frame scale. *GPS Solut.* **2022**, *26*, 109. [CrossRef]
54. Li, R.; Wang, N.; Li, Z.; Zhang, Y.; Wang, Z.; Ma, H. Precise orbit determination of BDS-3 satellites using B1C and B2a dual-frequency measurements. *GPS Solut.* **2021**, *25*, 1–14. [CrossRef]